**Electronic Supplementary Information**

# Fluorescence excitation and dispersed fluorescence spectra of *iso*-quinolinyl radicals 4-, 5, and 8-*iso*-$HC_9H_7N$ isolated in solid *para*-Hydrogen

*Chun-Kai Chen,*[†] *Isabelle Weber,*[†*] *Qin Yang*[‡] *and Yuan-Pern Lee*[†,§*]

[†] Department of Applied Chemistry and Institute of Molecular Science, National Yang Ming Chiao Tung University, Hsinchu 3000093, Taiwan

[‡] Institute of Organic Chemistry and Biochemistry, Academy of Sciences, Flemingovonáměstú 2, 16610 Prague, Czech Republic

[§] Center for Emergent Functional Matter Science, National Yang Ming Chiao Tung University, Hsinchu 300093, Taiwan

**Table of Contents**

**Section SA. Variations in vibronic patterns as a function of the position of H-addition**

Although the vibronic patterns vary considerably depending on the position of H-addition as shown in Figs. 2(d)−2(j) of the main manuscript, several trends emerge. A qualitative explanation of these trends is attempted in this section.

First, the simulated $D_1 \rightarrow D_0$ spectra of isomers hydrogenated at the C atom adjacent to the bridging C atoms, namely, 4-, 5-, and 8-*iso*-$HC_9H_7N$, consistently exhibit a characteristic feature near 615 $cm^{-1}$, corresponding to $\nu_{29}$ (*a*'), the out-of-phase CCC/CCN bending motion of both rings. In contrast, this feature does not appear in the simulated emission spectra of 3-, 6-, and 7-*iso*-$C_9H_7N$, which instead display a characteristic feature near 503 $cm^{-1}$, corresponding to $\nu_{30}$ (*a*'), an in-phase CCC/CCN bending motion of both rings inducing a diagonal elongation of the molecular framework. In the spectra of 3- and 6-*iso*-$HC_9H_7N$, this feature is accompanied by a second contribution of comparable intensity corresponding to $\nu_{31}$ (*a*'), the in-phase deformation of both rings along the minor axis of the molecular plane. Additionally, the simulated spectra of 3-, 5-, and 7-*iso*-$HC_9H_7N$ exhibit a characteristic feature near 345 $cm^{-1}$, associated with $\nu_{32}$ (*a*'), the scissoring motion of the two ring moieties.

Atomic vector displacements corresponding to the four in-plane skeletal deformation modes, $\nu_{29}$, $\nu_{30}$, $\nu_{31}$, and $\nu_{32}$, are schematically illustrated in Fig. S3 (ESI†). Geometry changes in the ring moiety induced by the electronic transition from $D_0$ to $D_1$ are depicted in Fig. S4 (ESI†) for all *iso*-$HC_9H_7N$ isomers included in Fig. 2 of the main manuscript, except for *iso*-$C_9H_7NH$. In 4-, 5-, and 8-*iso*-$HC_9H_7N$, $D_0 \rightarrow D_1$ transition induces elongation of three parallel C−C/C−N bonds: N−C(3), C(4*a*)−C(8*a*), and C(6)−C(7). Conversely, in 3-, 6-, and 7-*iso*-$C_9H_7N$, at least one of these bonds is shortened, resulting in a diagonal deformation of the ring moiety similar to the atomic vector displacements characteristic for $\nu_{30}$ (*a*'). This diagonal distortion is most pronounced in 7-*iso*-$HC_9H_7N$, consistent with the significantly greater contribution of $\nu_{30}$ (*a*') relative to $\nu_{31}$ (*a*') in the vibronic stick spectrum. In contrast, the deformation is less evident in 3- and 6-*iso*-$HC_9H_7N$, in line with the increased contribution of $\nu_{31}$ (*a*').

Changes in the outer angles at the bridging C-atoms, i.e. ∠C(4)C(4*a*)C(5) and ∠C(8)C(8*a*)C(1), correlate with the contribution of the ring scissoring vibration $\nu_{32}$ (*a*') to the vibronic spectra. For 6- and 8-*iso*-$HC_9H_7N$, the changes of these two angles upon $D_0 \rightarrow D_1$ transition are comparable, and thus $\nu_{32}$ (*a*') is not expected to contribute significantly. In contrast, 3-, 5-, and 7-*iso*-$HC_9H_7N$ exhibit pronounced differences in these two angles, resulting in a scissoring motion and consequently notably intensity in $\nu_{32}$ (*a*'). The stick

spectrum of 4-*iso*-$HC_9H_7N$ exhibits only a weak contribution from $\nu_{32}$ (*a*'), consistent with the smaller disparity in bond angle changes compared to 3-, 5-, and 7-*iso*-$HC_9H_7N$.

Second, the in-plane C−H bending modes near 1420 $cm^{-1}$, i.e. $\nu_{13}$ (*a*') and $\nu_{15}$ (*a*'), carry notable intensity only in the emission spectra of 6-*iso*-$HC_9H_7N$ and *iso*-$C_9H_7NH$. These modes not only impact various CCH-angles but also affect the bond lengths of three consecutive bonds adjacent to the hydrogenation site. For 6-*iso*-$HC_9H_7N$, the impacted bonds are C(4*a*)−C(5), C(4*a*)−C(8*a*), and C(8)−C(8*a*), the latter two of which are strongly influenced by the $D_1$−$D_0$ transition.

Finally, across all spectra, at least one of the three C−C stretching modes, $\nu_8$ (*a*'), $\nu_9$ (*a*'), and $\nu_{10}$ (*a*'), in the region 1500−1700 $cm^{-1}$ carries notable intensity; differences in the intensity pattern of these modes for the three experimentally observed isomers are discussed in in sections 3.2 and 3.5 of the main manuscript.

**Table S1** Scaled harmonic vibrational wavenumbers of the electronic ground ($D_0$) state and the first electronic excited ($D_1$) state of 1-*iso*-$HC_9H_7N$, *iso*-$C_9H_7NH$, and 3-*iso*-$HC_9H_7N$ calculated with the (TD-)uB3PW91/6-311++G(2d,2p) method

| Mode | Sym. | 1-*iso*-$HC_9H_7N$ | | | *iso*-$C_9H_7NH$ | | | 3-*iso*-$HC_9H_7N$ | | |
|---|---|---|---|---|---|---|---|---|---|---|
| | | $D_0$ | | $D_1$ | $D_0$ | | $D_1$ | $D_0$ | | $D_1$ |
| | | scaled[a] | IR int.[b] | scaled[a,c] | scaled[a,c] | IR int.[b] | scaled[a,c] | scaled[a] | IR int.[b] | scaled[a] |
| $\nu_1$ | *a*' | 3132 | (31) | 3161 | 3610 | (100) | 3574 | 3134 | (25) | 3150 |
| $\nu_2$ | *a*' | 3125 | (32) | 3133 | 3165 | (4) | 3202 | 3120 | (32) | 3124 |
| $\nu_3$ | *a*' | 3118 | (50) | 3119 | 3151 | (8) | 3143 | 3106 | (4) | 3106 |
| $\nu_4$ | *a*' | 3106 | (8) | 3106 | 3133 | (9) | 3136 | 3103 | (20) | 3099 |
| $\nu_5$ | *a*' | 3096 | (10) | 3101 | 3132 | (6) | 3124 | 3100 | (10) | 3098 |
| $\nu_6$ | *a*' | 3055 | (47) | 3078 | 3115 | (21) | 3115 | 3026 | (59) | 3084 |
| $\nu_7$ | *a*' | 2921 | (51) | 3016 | 3101 | (5) | 3097 | 2900 | (69) | 2871 |
| $\nu_8$ | *a*' | 1599 | (45) | 2851 | 3097 | (8) | 3092 | 1648 | (100) | 1652 |
| $\nu_9$ | *a*' | 1571 | (23) | 1605 | 1613 | (45) | 2239 | 1575 | (9) | 1518 |
| $\nu_{10}$ | *a*' | 1515 | (12) | 1575 | 1580 | (17) | 1603 | 1542 | (21) | 1513 |
| $\nu_{11}$ | *a*' | 1482 | (6) | 1555 | 1546 | (6) | 1567 | 1477 | (1) | 1486 |
| $\nu_{12}$ | *a*' | 1441 | (28) | 1487 | 1487 | (13) | 1514 | 1441 | (3) | 1440 |
| $\nu_{13}$ | *a*' | 1404 | (33) | 1466 | 1482 | (20) | 1500 | 1416 | (2) | 1392 |
| $\nu_{14}$ | *a*' | 1343 | (8) | 1443 | 1439 | (17) | 1462 | 1394 | (11) | 1361 |
| $\nu_{15}$ | *a*' | 1331 | (2) | 1422 | 1418 | (10) | 1388 | 1370 | (6) | 1329 |
| $\nu_{16}$ | *a*' | 1287 | (7) | 1340 | 1391 | (6) | 1379 | 1328 | (4) | 1266 |
| $\nu_{17}$ | *a*' | 1250 | (10) | 1317 | 1324 | (3) | 1348 | 1308 | (2) | 1261 |
| $\nu_{18}$ | *a*' | 1214 | (9) | 1281 | 1266 | (3) | 1280 | 1260 | (10) | 1249 |
| $\nu_{19}$ | *a*' | 1212 | (5) | 1267 | 1226 | (0) | 1264 | 1224 | (27) | 1221 |
| $\nu_{20}$ | *a*' | 1184 | (23) | 1215 | 1202 | (3) | 1236 | 1179 | (16) | 1188 |
| $\nu_{21}$ | *a*' | 1150 | (3) | 1194 | 1182 | (23) | 1208 | 1138 | (9) | 1157 |
| $\nu_{22}$ | *a*' | 1116 | (1) | 1160 | 1141 | (4) | 1164 | 1114 | (9) | 1106 |
| $\nu_{23}$ | *a*' | 1067 | (4) | 1154 | 1126 | (1) | 1143 | 1037 | (21) | 1064 |
| $\nu_{24}$ | *a*' | 1034 | (9) | 1111 | 1111 | (9) | 1104 | 1019 | (8) | 1015 |
| $\nu_{25}$ | *a*' | 955 | (7) | 1102 | 1026 | (6) | 990 | 934 | (1) | 920 |
| $\nu_{26}$ | *a*' | 917 | (14) | 1034 | 988 | (79) | 963 | 875 | (63) | 893 |
| $\nu_{27}$ | *a*' | 786 | (6) | 982 | 930 | (3) | 946 | 773 | (13) | 772 |
| $\nu_{28}$ | *a*' | 749 | (8) | 967 | 790 | (3) | 913 | 745 | (1) | 736 |
| $\nu_{29}$ | *a*' | 607 | (4) | 952 | 752 | (0) | 911 | 614 | (5) | 605 |
| $\nu_{30}$ | *a*' | 505 | (0) | 929 | 611 | (0) | 875 | 500 | (0) | 503 |
| $\nu_{31}$ | *a*' | 469 | (2) | 895 | 505 | (0) | 834 | 483 | (1) | 472 |
| $\nu_{32}$ | *a*' | 341 | (0) | 884 | 491 | (0) | 782 | 341 | (0) | 342 |
| $\nu_{33}$ | *a*' | 2928 | (18) | 847 | 352 | (3) | 771 | 2896 | (18) | 2865 |
| $\nu_{34}$ | *a*" | 1393 | (1) | 783 | 945 | (0) | 735 | 1203 | (2) | 1118 |
| $\nu_{35}$ | *a*" | 973 | (1) | 751 | 911 | (1) | 713 | 967 | (16) | 967 |
| $\nu_{36}$ | *a*" | 970 | (3) | 745 | 899 | (4) | 681 | 964 | (3) | 896 |
| $\nu_{37}$ | *a*" | 941 | (3) | 712 | 822 | (0) | 634 | 930 | (0) | 857 |
| $\nu_{38}$ | *a*" | 911 | (3) | 709 | 757 | (32) | 623 | 904 | (2) | 837 |
| $\nu_{39}$ | *a*" | 847 | (60) | 607 | 734 | (73) | 545 | 839 | (1) | 778 |

| | | | | | | | | | | |
|---|---|---|---|---|---|---|---|---|---|---|
| $\nu_{40}$ | *a*" | 768 | (5) | 563 | 707 | (9) | 510 | 745 | (89) | 735 |
| $\nu_{41}$ | *a*" | 708 | (33) | 497 | 592 | (4) | 482 | 725 | (40) | 693 |
| $\nu_{42}$ | *a*" | 700 | (100) | 470 | 573 | (12) | 427 | 666 | (0) | 661 |
| $\nu_{43}$ | *a*" | 524 | (7) | 450 | 475 | (14) | 410 | 537 | (11) | 464 |
| $\nu_{44}$ | *a*" | 459 | (16) | 408 | 425 | (2) | 345 | 447 | (45) | 421 |
| $\nu_{45}$ | *a*" | 415 | (15) | 351 | 321 | (22) | 325 | 395 | (3) | 297 |
| $\nu_{46}$ | *a*" | 238 | (4) | 275 | 280 | (43) | 184 | 240 | (0) | 231 |
| $\nu_{47}$ | *a*" | 166 | (1) | 175 | 175 | (9) | 166 | 165 | (0) | 146 |
| $\nu_{48}$ | *a*" | 71 | (1) | 125 | 146 | (0) | 87 | 105 | (5) | 124 |

[a]Harmonic vibrational wavenumbers scaled by 0.978. [b]IR intensity relative to the most intense mode, i.e. $\nu_{42}$ (56 km mol$^{-1}$) for 1-*iso*-$HC_9H_7N$, $\nu_1$ (110 km mol$^{-1}$) for *iso*-$C_9H_7NH$, and $\nu_8$ (53 km/mol) for 3-*iso*-$HC_9H_7N$. [c]Symmetry elements do not apply; vibrational normal modes listed in descending order.

**Table S2** Scaled harmonic vibrational wavenumbers of the electronic ground ($D_0$) state and the first electronic excited ($D_1$) state of 4-, 5-, and 6-*iso*-$HC_9H_7N$ calculated with the (TD-) uB3PW91/6-311++G(2d,2p) method

| Mode | Sym. | 4-*iso*-$HC_9H_7N$ | | | 5-*iso*-$HC_9H_7N$ | | | 6-*iso*-$HC_9H_7N$ | | |
|---|---|---|---|---|---|---|---|---|---|---|
| | | $D_0$ | | $D_1$ | $D_0$ | | $D_1$ | $D_0$ | | $D_1$ |
| | | scaled[a] | IR int.[b] | scaled[a] | scaled[a] | IR int.[b] | scaled[a] | scaled[a] | IR int.[b] | scaled[a] |
| $\nu_1$ | *a*' | 3132 | (22) | 3137 | 3129 | (31) | 3139 | 3119 | (51) | 3131 |
| $\nu_2$ | *a*' | 3118 | (26) | 3123 | 3119 | (32) | 3124 | 3115 | (66) | 3119 |
| $\nu_3$ | *a*' | 3105 | (5) | 3103 | 3111 | (50) | 3113 | 3107 | (26) | 3110 |
| $\nu_4$ | *a*' | 3101 | (14) | 3099 | 3101 | (8) | 3095 | 3095 | (10) | 3106 |
| $\nu_5$ | *a*' | 3097 | (9) | 3096 | 3092 | (10) | 3092 | 3092 | (41) | 3101 |
| $\nu_6$ | *a*' | 3070 | (34) | 3064 | 3074 | (47) | 3049 | 3072 | (71) | 3070 |
| $\nu_7$ | *a*' | 2914 | (37) | 2912 | 2913 | (51) | 2902 | 2888 | (100) | 2880 |
| $\nu_8$ | *a*' | 1602 | (1) | 1624 | 1587 | (45) | 1585 | 1642 | (10) | 1703 |
| $\nu_9$ | *a*' | 1576 | (2) | 1532 | 1561 | (23) | 1522 | 1564 | (75) | 1501 |
| $\nu_{10}$ | *a*' | 1513 | (15) | 1492 | 1522 | (12) | 1472 | 1521 | (7) | 1469 |
| $\nu_{11}$ | *a*' | 1486 | (19) | 1428 | 1490 | (6) | 1458 | 1451 | (72) | 1435 |
| $\nu_{12}$ | *a*' | 1445 | (15) | 1414 | 1425 | (28) | 1409 | 1432 | (13) | 1421 |
| $\nu_{13}$ | *a*' | 1406 | (19) | 1383 | 1406 | (33) | 1378 | 1417 | (17) | 1399 |
| $\nu_{14}$ | *a*' | 1369 | (2) | 1356 | 1404 | (8) | 1370 | 1397 | (31) | 1374 |
| $\nu_{15}$ | *a*' | 1346 | (2) | 1335 | 1359 | (2) | 1340 | 1379 | (18) | 1367 |
| $\nu_{16}$ | *a*' | 1320 | (6) | 1313 | 1314 | (7) | 1316 | 1336 | (22) | 1318 |
| $\nu_{17}$ | *a*' | 1277 | (24) | 1299 | 1285 | (10) | 1277 | 1280 | (31) | 1298 |
| $\nu_{18}$ | *a*' | 1247 | (31) | 1257 | 1254 | (9) | 1247 | 1265 | (14) | 1254 |
| $\nu_{19}$ | *a*' | 1217 | (7) | 1215 | 1213 | (5) | 1192 | 1229 | (2) | 1230 |
| $\nu_{20}$ | *a*' | 1183 | (5) | 1151 | 1198 | (23) | 1167 | 1185 | (16) | 1181 |
| $\nu_{21}$ | *a*' | 1151 | (0) | 1130 | 1167 | (3) | 1142 | 1157 | (17) | 1172 |
| $\nu_{22}$ | *a*' | 1140 | (3) | 1125 | 1148 | (1) | 1098 | 1149 | (4) | 1090 |
| $\nu_{23}$ | *a*' | 1113 | (1) | 1026 | 1072 | (4) | 1050 | 1049 | (14) | 1037 |
| $\nu_{24}$ | *a*' | 1034 | (4) | 959 | 1052 | (9) | 966 | 1028 | (5) | 979 |
| $\nu_{25}$ | *a*' | 940 | (8) | 950 | 938 | (7) | 923 | 916 | (16) | 889 |
| $\nu_{26}$ | *a*' | 899 | (7) | 862 | 906 | (14) | 811 | 888 | (70) | 863 |
| $\nu_{27}$ | *a*' | 780 | (12) | 755 | 787 | (6) | 766 | 773 | (20) | 754 |
| $\nu_{28}$ | *a*' | 748 | (2) | 713 | 751 | (8) | 711 | 759 | (3) | 742 |
| $\nu_{29}$ | *a*' | 612 | (3) | 604 | 617 | (4) | 599 | 617 | (13) | 610 |
| $\nu_{30}$ | *a*' | 504 | (1) | 496 | 499 | (0) | 488 | 503 | (1) | 492 |
| $\nu_{31}$ | *a*' | 475 | (1) | 464 | 471 | (2) | 462 | 481 | (1) | 390 |
| $\nu_{32}$ | *a*' | 344 | (0) | 336 | 345 | (0) | 334 | 344 | (0) | 330 |
| $\nu_{33}$ | *a*" | 2921 | (12) | 2922 | 2919 | (18) | 2909 | 2883 | (27) | 2871 |
| $\nu_{34}$ | *a*" | 1162 | (1) | 1067 | 1175 | (1) | 1083 | 1155 | (2) | 1124 |
| $\nu_{35}$ | *a*" | 972 | (0) | 951 | 961 | (1) | 968 | 976 | (2) | 911 |
| $\nu_{36}$ | *a*" | 948 | (2) | 929 | 944 | (3) | 923 | 965 | (0) | 888 |
| $\nu_{37}$ | *a*" | 920 | (2) | 894 | 929 | (3) | 900 | 923 | (16) | 859 |
| $\nu_{38}$ | *a*" | 856 | (1) | 813 | 911 | (3) | 844 | 898 | (38) | 802 |
| $\nu_{39}$ | *a*" | 789 | (21) | 768 | 821 | (60) | 785 | 809 | (98) | 770 |

| | | | | | | | | | |
|---|---|---|---|---|---|---|---|---|---|
| $\nu_{40}$ | *a*" | 742 | (100) | 691 | 767 | (5) | 765 | 785 | (9) | 723 |
| $\nu_{41}$ | *a*" | 714 | (0) | 618 | 712 | (33) | 618 | 699 | (66) | 675 |
| $\nu_{42}$ | *a*" | 683 | (0) | 569 | 645 | (100) | 608 | 683 | (22) | 559 |
| $\nu_{43}$ | *a*" | 524 | (9) | 415 | 543 | (7) | 437 | 546 | (0) | 514 |
| $\nu_{44}$ | *a*" | 477 | (8) | 345 | 468 | (16) | 371 | 449 | (65) | 382 |
| $\nu_{45}$ | *a*" | 420 | (5) | 313 | 399 | (15) | 287 | 369 | (0) | 292 |
| $\nu_{46}$ | *a*" | 232 | (4) | 178 | 243 | (4) | 202 | 252 | (5) | 232 |
| $\nu_{47}$ | *a*" | 166 | (2) | 114 | 167 | (1) | 147 | 168 | (3) | 150 |
| $\nu_{48}$ | *a*" | 56 | (3) | 26 | 86 | (1) | 95 | 124 | (0) | 117 |

[a]Harmonic vibrational wavenumbers scaled by 0.978. [b]IR intensity relative to the most intense mode, i.e. $\nu_{40}$ (65 km/mol) for 4-*iso*-$HC_9H_7N$, $\nu_{42}$ (42 km/mol) for 5-*iso*-$HC_9H_7N$, and $\nu_7$ (33 km/mol) for 6-*iso*-$HC_9H_7N$.

**Table S3** Scaled harmonic vibrational wavenumbers of the electronic ground ($D_0$) state and the first electronic excited ($D_1$) state of 6-, 7-, and 8-*iso*-$HC_9H_7N$ calculated with the (TD-) uB3PW91/6-311++G(2d,2p) method

| Mode | Sym. | 7-*iso*-$HC_9H_7N$ | | | 8-*iso*-$HC_9H_7N$ | | |
|---|---|---|---|---|---|---|---|
| | | $D_0$ | | $D_1$ | $D_0$ | | $D_1$ |
| | | scaled[a] | IR int.[b] | scaled[a] | scaled[a] | IR int.[b] | scaled[a] |
| $\nu_1$ | *a*' | 3117 | (56) | 3148 | 3130 | (26) | 3148 |
| $\nu_2$ | *a*' | 3114 | (36) | 3124 | 3119 | (54) | 3125 |
| $\nu_3$ | *a*' | 3107 | (31) | 3112 | 3118 | (6) | 3123 |
| $\nu_4$ | *a*' | 3098 | (12) | 3107 | 3101 | (6) | 3103 |
| $\nu_5$ | *a*' | 3094 | (7) | 3080 | 3090 | (33) | 3100 |
| $\nu_6$ | *a*' | 3070 | (45) | 3068 | 3066 | (45) | 3058 |
| $\nu_7$ | *a*' | 2887 | (98) | 2895 | 2913 | (33) | 2907 |
| $\nu_8$ | *a*' | 1644 | (6) | 1677 | 1590 | (100) | 1604 |
| $\nu_9$ | *a*' | 1557 | (86) | 1519 | 1558 | (8) | 1539 |
| $\nu_{10}$ | *a*' | 1517 | (11) | 1512 | 1528 | (5) | 1464 |
| $\nu_{11}$ | *a*' | 1473 | (7) | 1449 | 1473 | (30) | 1441 |
| $\nu_{12}$ | *a*' | 1436 | (21) | 1430 | 1431 | (35) | 1405 |
| $\nu_{13}$ | *a*' | 1408 | (6) | 1407 | 1409 | (13) | 1397 |
| $\nu_{14}$ | *a*' | 1404 | (16) | 1383 | 1404 | (10) | 1369 |
| $\nu_{15}$ | *a*' | 1366 | (13) | 1338 | 1368 | (2) | 1333 |
| $\nu_{16}$ | *a*' | 1334 | (9) | 1310 | 1316 | (10) | 1323 |
| $\nu_{17}$ | *a*' | 1287 | (19) | 1293 | 1273 | (5) | 1252 |
| $\nu_{18}$ | *a*' | 1260 | (6) | 1260 | 1264 | (29) | 1233 |
| $\nu_{19}$ | *a*' | 1228 | (1) | 1228 | 1215 | (6) | 1172 |
| $\nu_{20}$ | *a*' | 1204 | (23) | 1200 | 1184 | (3) | 1169 |
| $\nu_{21}$ | *a*' | 1151 | (1) | 1180 | 1173 | (6) | 1143 |
| $\nu_{22}$ | *a*' | 1142 | (5) | 1090 | 1150 | (0) | 1065 |
| $\nu_{23}$ | *a*' | 1051 | (5) | 1036 | 1071 | (5) | 1045 |
| $\nu_{24}$ | *a*' | 1016 | (9) | 1025 | 1056 | (5) | 986 |
| $\nu_{25}$ | *a*' | 912 | (16) | 920 | 936 | (31) | 924 |
| $\nu_{26}$ | *a*' | 887 | (29) | 896 | 910 | (12) | 877 |
| $\nu_{27}$ | *a*' | 775 | (6) | 768 | 784 | (16) | 752 |
| $\nu_{28}$ | *a*' | 754 | (7) | 739 | 757 | (0) | 690 |
| $\nu_{29}$ | *a*' | 621 | (9) | 612 | 616 | (5) | 587 |
| $\nu_{30}$ | *a*' | 494 | (4) | 496 | 499 | (5) | 485 |
| $\nu_{31}$ | *a*' | 485 | (3) | 471 | 472 | (3) | 463 |
| $\nu_{32}$ | *a*' | 343 | (0) | 346 | 345 | (0) | 336 |
| $\nu_{33}$ | *a*" | 2881 | (26) | 2896 | 2919 | (13) | 2914 |
| $\nu_{34}$ | *a*" | 1160 | (1) | 1072 | 1173 | (1) | 1097 |
| $\nu_{35}$ | *a*" | 979 | (1) | 977 | 973 | (0) | 943 |
| $\nu_{36}$ | *a*" | 938 | (6) | 887 | 949 | (3) | 923 |
| $\nu_{37}$ | *a*" | 909 | (17) | 836 | 943 | (0) | 911 |
| $\nu_{38}$ | *a*" | 902 | (12) | 827 | 891 | (2) | 807 |
| $\nu_{39}$ | *a*" | 819 | (100) | 768 | 831 | (71) | 764 |

| | | | | | | | |
|---|---|---|---|---|---|---|---|
| $\nu_{40}$ | *a*" | 784 | (2) | 740 | 773 | (2) | 734 |
| $\nu_{41}$ | *a*" | 694 | (0) | 670 | 719 | (3) | 619 |
| $\nu_{42}$ | *a*" | 678 | (27) | 542 | 648 | (78) | 587 |
| $\nu_{43}$ | *a*" | 553 | (65) | 464 | 545 | (18) | 419 |
| $\nu_{44}$ | *a*" | 434 | (18) | 390 | 450 | (0) | 389 |
| $\nu_{45}$ | *a*" | 380 | (3) | 301 | 408 | (20) | 298 |
| $\nu_{46}$ | *a*" | 246 | (0) | 214 | 244 | (2) | 201 |
| $\nu_{47}$ | *a*" | 167 | (0) | 146 | 168 | (3) | 150 |
| $\nu_{48}$ | *a*" | 119 | (3) | 126 | 85 | (3) | 95 |

[a]Harmonic vibrational wavenumbers scaled by 0.978. [b]IR intensity relative to the most intense mode, i.e. $\nu_{39}$ (42 km/mol) for 7-*iso*-$HC_9H_7N$ and $\nu_8$ (51 km/mol) for 8-*iso*-$HC_9H_7N$.

**Fig. S1** Side-views of the optimized geometry of the $D_1$ state of 1-*iso*-$HC_9H_7N$ radical computed with the TD-uB3PW91/6-311++G(2d,2p) method. H atoms are in white, C atoms in grey and the N atom in blue.

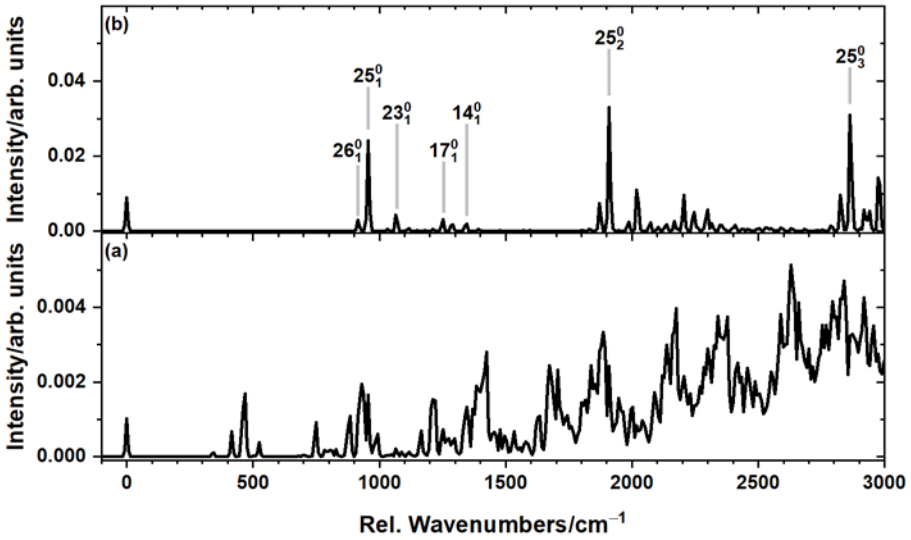


**Fig. S2** $D_1 \rightarrow D_0$ emission spectra of 1-*iso*-$HC_9H_7N$ obtained from Franck-Condon Herzberg-Teller simulations based on ground and excited state geometries and harmonic vibrational frequencies calculated at the (TD-)uB3PW91/6-311++G(2d,2p) level. To increase the convergence of the simulation, the dimensionality of vibrational normal modes was reduced by (a) four and (b) ten using a block definition threshold of 0.75. Key fundamental normal modes are labeled. The consecutive groups of peaks consist of combinations of these fundamentals with $\nu_{25}$ and $\nu_{25}$ overtones.

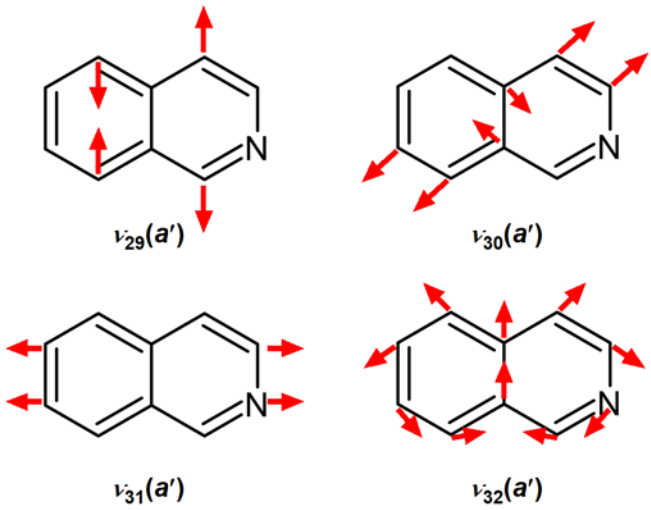


**Fig. S3** Characteristic atomic displacement vectors induced by the four ring-deformation modes $\nu_{29}$, $\nu_{30}$, $\nu_{31}$, and $\nu_{32}$ in the $D_0$ state of *n*-*iso*-$HC_9H_7N$ ($n$ = 3−8).

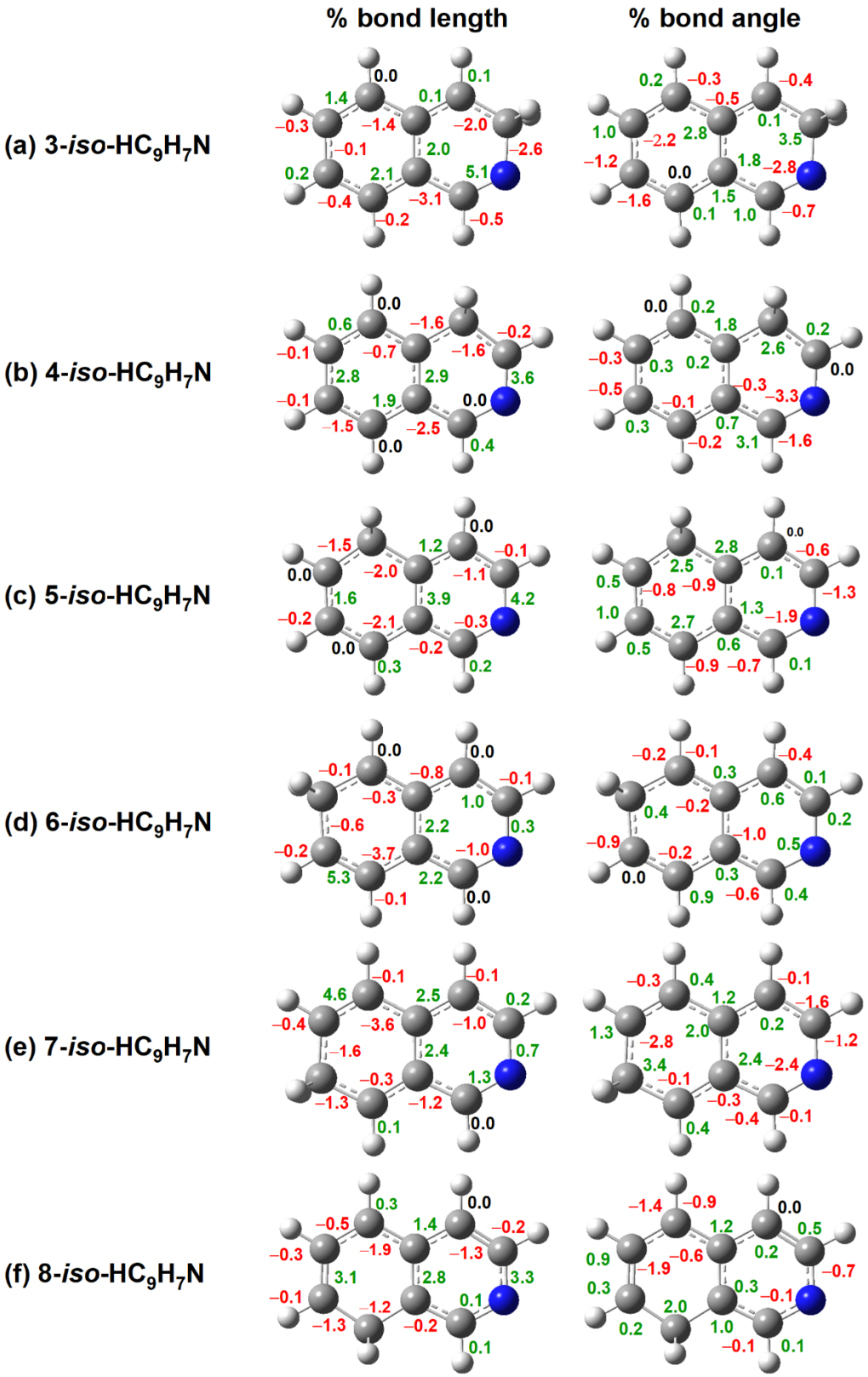


**Fig. S4** Relative percentage changes of bond lengths and angles between the optimized geometries of the electronic ground state ($D_0$) and the first electronic excited state ($D_1$) of various *iso*-$HC_9H_7N$ isomers. Negative values (red) correspond to a decrease, positive values (green) to an increase of the respective observable upon transition to the excited state.

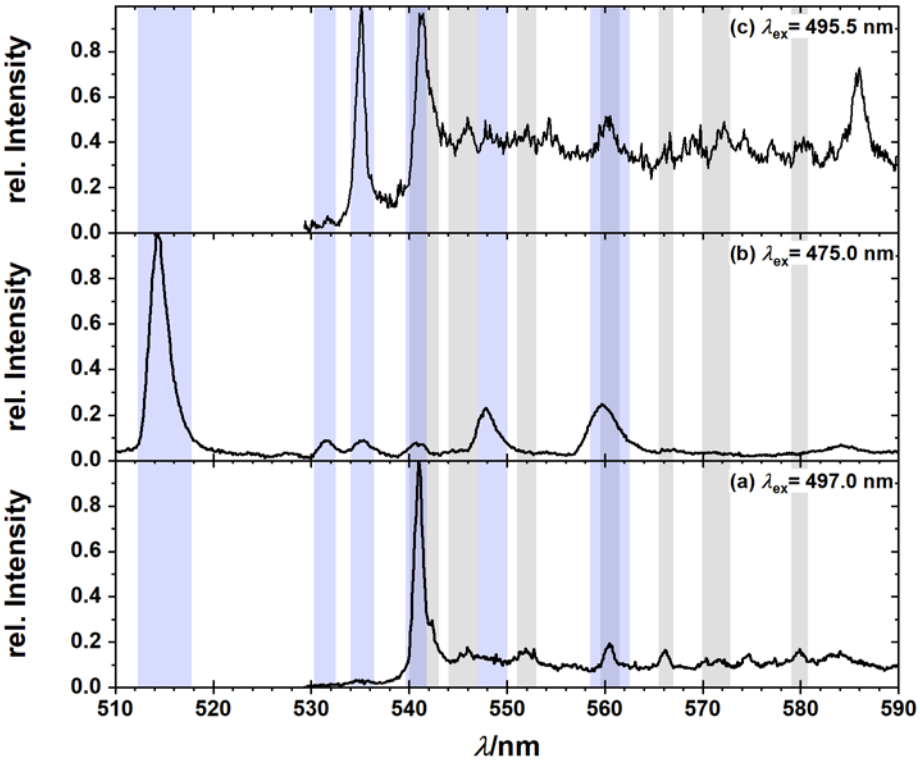


**Fig. S5** Partial dispersed fluorescence spectra of *iso*-$C_9H_7N$/*para*-$H_2$ deposited under electron bombardment upon excitation at (a) 497.0 nm, (b) 475.0 nm, and (c) 495.5 nm. Features assigned to 4-*iso*-$HC_9H_7N$ are shaded in grey, those assigned to 8-*iso*-$HC_9H_7N$ in blue. The additional unshaded features are assigned to 5-*iso*-$HC_9H_7N$. All spectra have been normalized to their most intense peak.

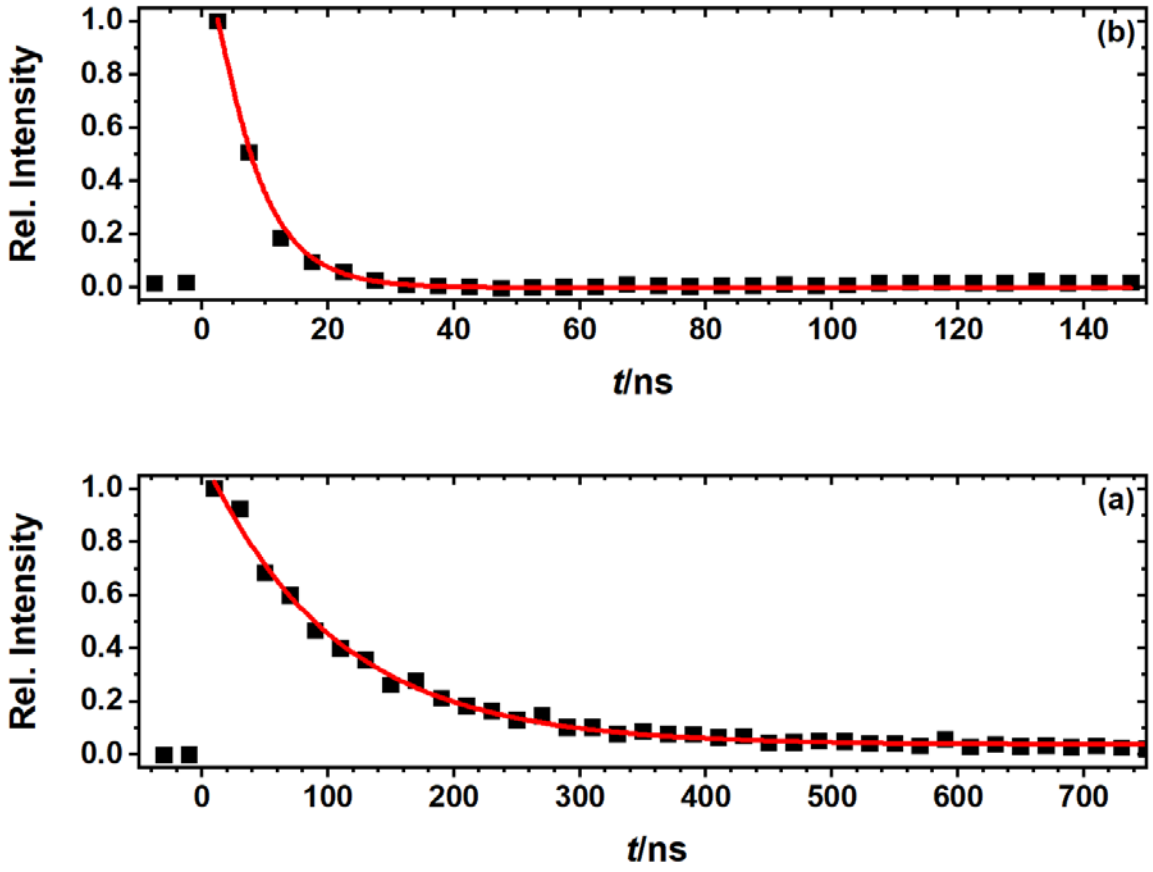


**Fig. S6** Temporal behavior of fluorescence emission of 4-*iso*-$HC_9H_7N$ and 8-*iso*-$HC_9H_7N$. (a) 4-*iso*-$HC_9H_7N$ probed in the range 587.2−596.7 nm (16759−17030 $cm^{-1}$) upon excitation at 540.8 nm (18491 $cm^{-1}$). Integration gate is 3 ns and acquisition interval is 5 ns. (b) 8-*iso*-$HC_9H_7N$ probed in the range 556.2−564.2 nm (17724−17979 $cm^{-1}$) upon excitation at 475.0 nm (21053 $cm^{-1}$). Integration gate is 15 ns and acquisition interval is 20 ns. The mono-exponential fit (red lines) gives fluorescence lifetimes of 6.6±0.3 ns for 4-*iso*-$HC_9H_7N$ (a) and 104±3 ns for 8-*iso*-$HC_9H_7N$ (b), respectively; errors correspond to one standard deviation in fitting.

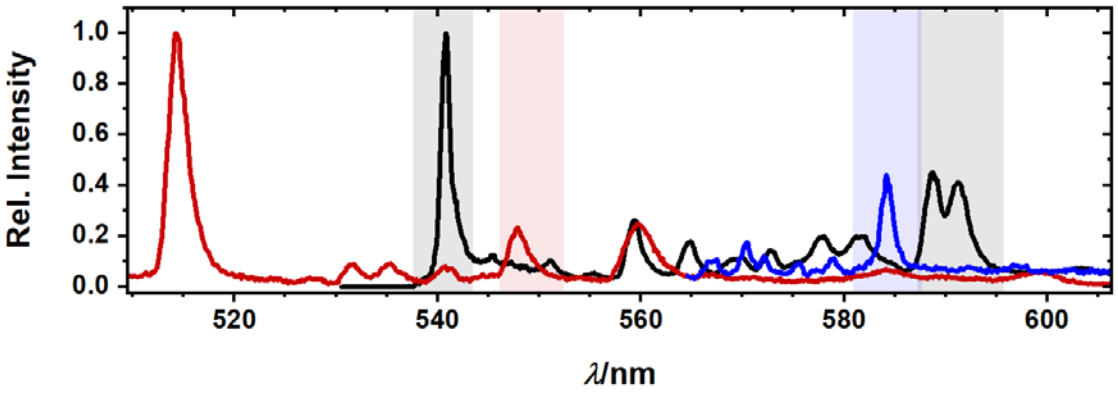


**Fig. S7** Normalized dispersed fluorescence spectra of 4-*iso*-$HC_9H_7N$ (black), 8-*iso*-$HC_9H_7N$ (red), and 5-*iso*-$HC_9H_7N$ (blue, partial) in solid *para*-$H_2$. The integration ranges selected to obtain the fluorescence excitation spectra of the three isomers shown in Figs. 5− 7 in the main manuscript are shaded in respective colors. The spectrum of 5-*iso*-$HC_9H_7N$ was normalized to match the predicted relative intensity of the band at 584 nm.

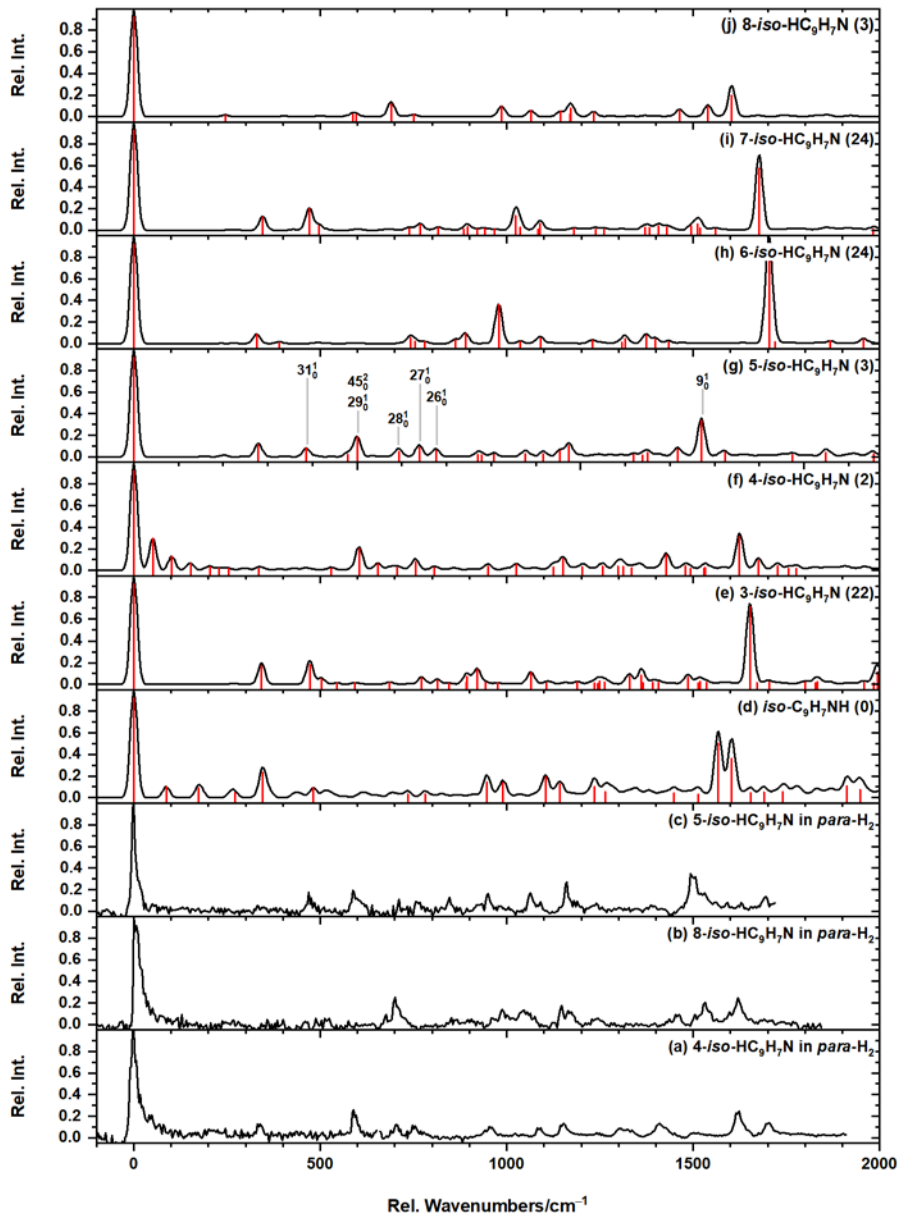


**Fig. S8** Comparison of observed fluorescence excitation spectra with simulated $D_1 \leftarrow D_0$ absorption spectra of various isomers of hydrogenated *iso*-quinoline. (a) 4-*iso*-$HC_9H_7N$, (b) 8-*iso*-$HC_9H_7N$, and (c) 5-*iso*-$HC_9H_7N$ isolated in solid *para*-$H_2$. Simulated absorption spectra of *iso*-$HC_9H_7N$ isomers are displayed in (d)−(j). To facilitate the comparison, we convoluted the computed Franck-Condon Herzberg-Teller stick spectra with a Gaussian lineshape of FWHM 20 $cm^{-1}$. Band assignments for peaks discussed in the main manuscript are provided. Relative energies in kJ $mol^{-1}$ are given in parentheses.

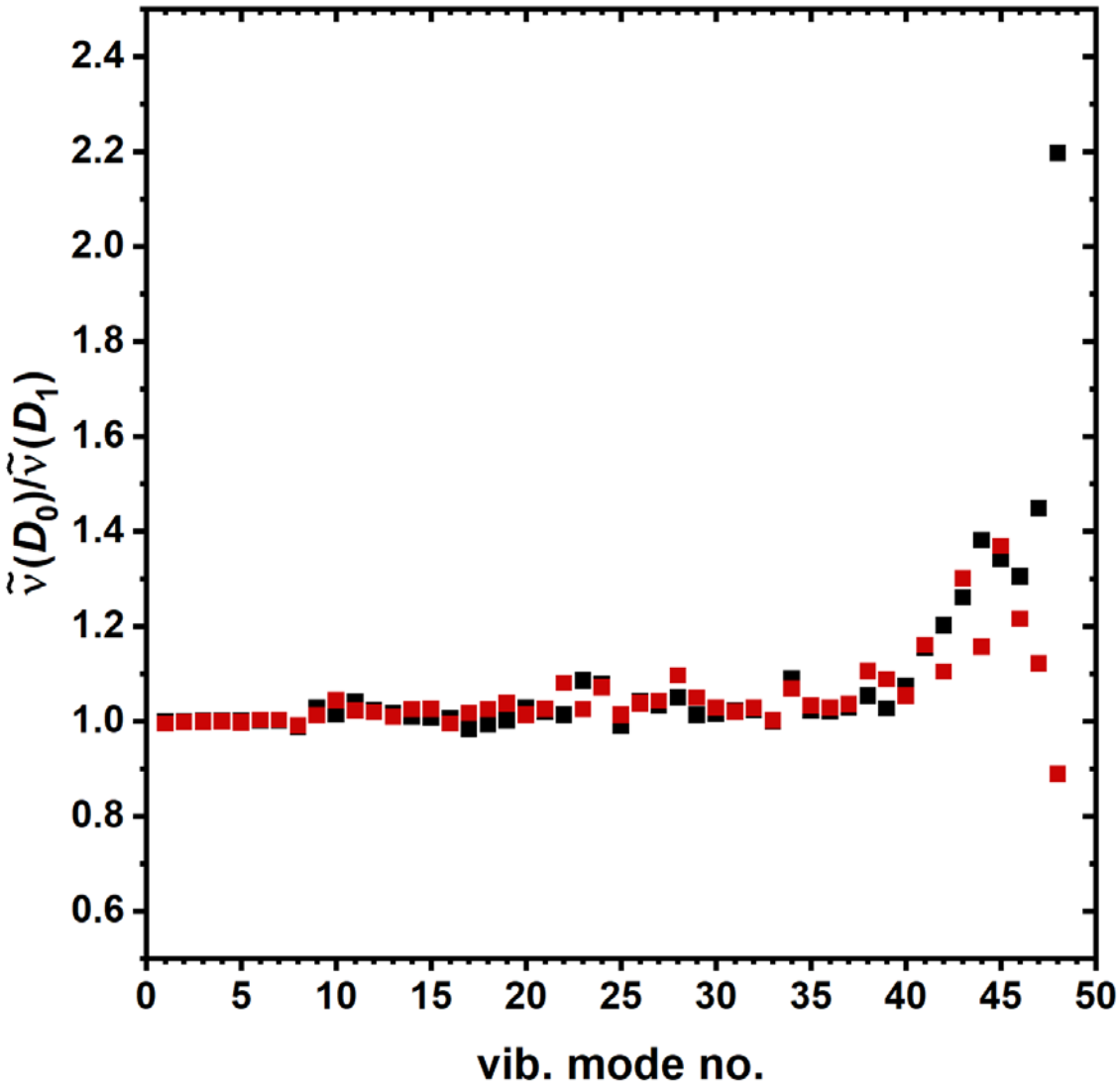


**Fig. S9** Quotient of vibrational wavenumbers of the electronic ground state ($D_0$) and the first electronic excited state ($D_1$) for 4-*iso*-$HC_9H_7N$ (black) and 8-*iso*-$HC_9H_7N$ (red).

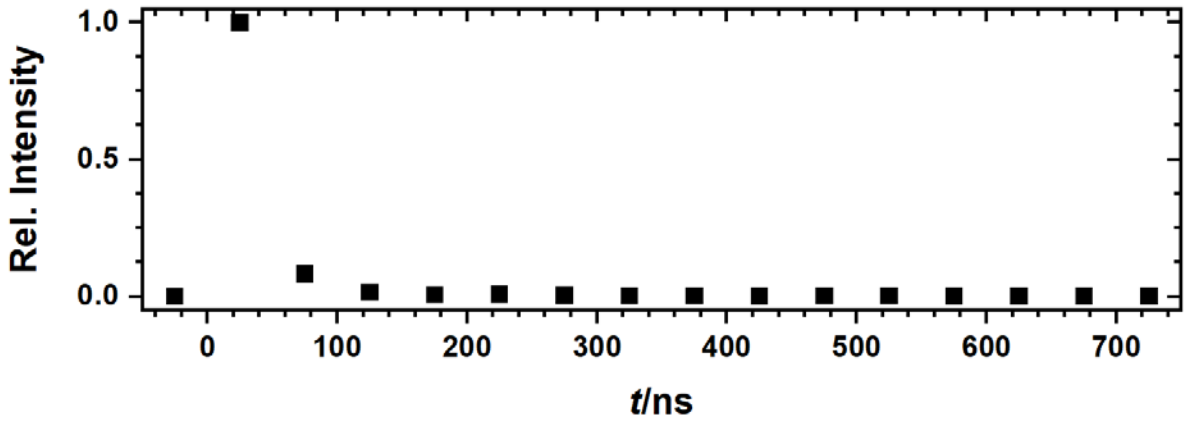


**Fig. S10** Temporal behavior of fluorescence emission of system C (5-*iso*-$HC_9H_7N$) probed in the range 580.9−587.6 nm (17018−17215 $cm^{-1}$) upon excitation at 535.1 nm (18688 $cm^{-1}$). Integration gate is 40 ns and acquisition interval is 50 ns.

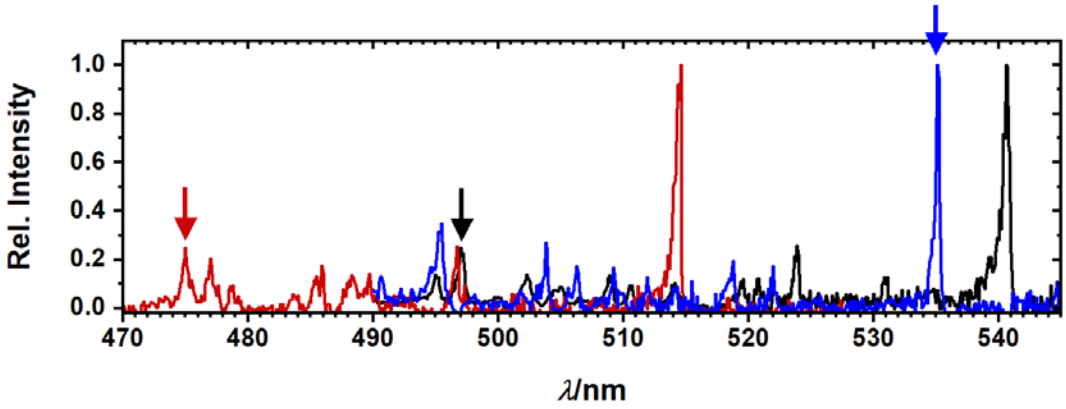


**Fig. S11** Normalized fluorescence excitation spectra of 4-*iso*-$HC_9H_7N$ (black), 8-*iso*-$HC_9H_7N$ (red), and 5-*iso*-$HC_9H_7N$ (blue) isolated in solid *para*-$H_2$. The excitation wavelength selected to obtain the dispersed fluorescence spectra of the three isomers shown in Figs. 4, 5, and 8 in the main manuscript are indicated by arrows. The integration ranges selected to obtain the fluorescence excitation spectra of the three isomers are shaded in respective colors in Fig. S7 (ESI†).

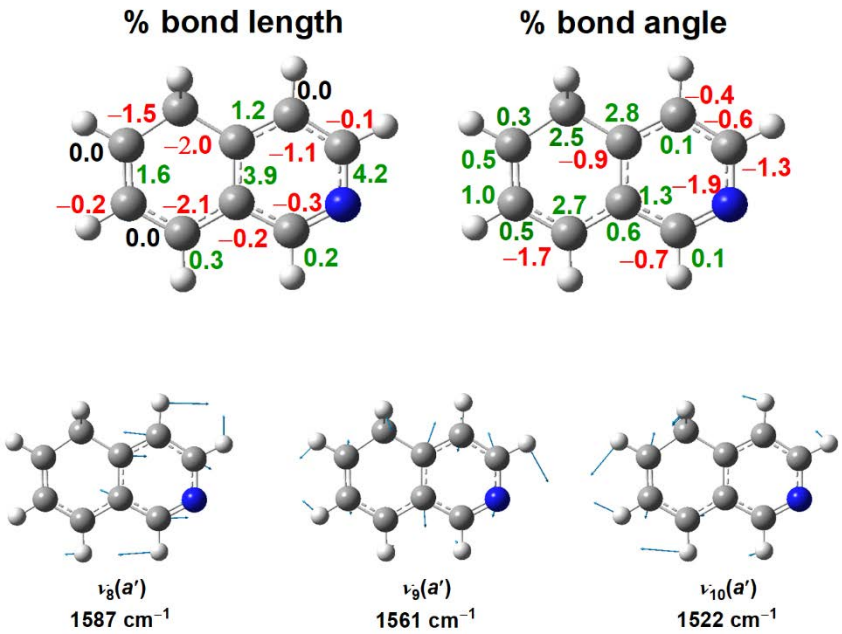


**Fig. S12** Changes in optimized geometries of 5-*iso*-$HC_9H_7N$ upon transition from $D_0$ to $D_1$ (top) and atomic displacement vectors induced by the three C−N and C−C stretching modes $\nu_8$, $\nu_9$, and $\nu_{10}$ in the electronic ground state (bottom). Negative values (red) correspond to a decrease, positive value (green) to an increase of the respective observable upon transition to the excited state.

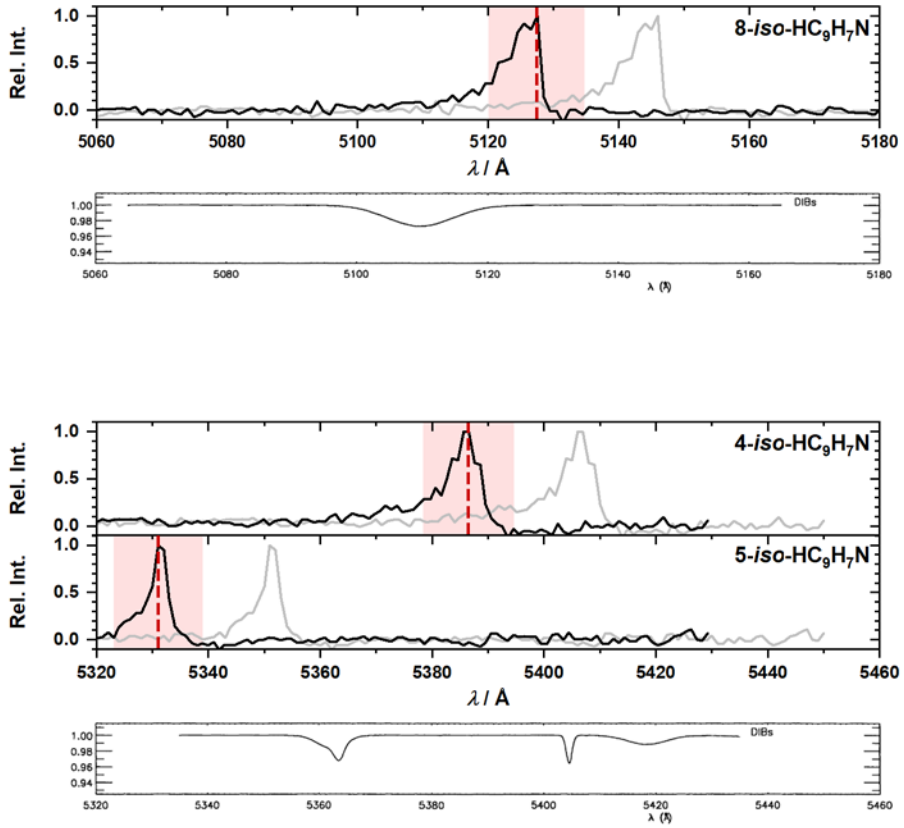


**Fig. S13** Comparison of the fluorescence excitation spectra of 4-, 5-, and 8-*iso*-$HC_9H_7N$ to the DIB spectrum reported by Jennsikens and Désert (Credit: P. Jenniskens, F.-X. Désert, A&A Suppl. Ser., 106, 39, 1994, reproduced with permission © ESO.). Gray curves represent observed excitation spectra in solid *para*-$H_2$ and black curves corresponding spectra corrected for matrix shift 70 $cm^{-1}$; the pink shaded regions indicate possible error ranges (±28 $cm^{-1}$) in the correction.